Detection and validation of hypoxia-related lncRNAs with associated ceRNA network involved in HCC prognosis, treatment responsiveness

Xiugai Li
China Medical University
Chang Zheng
The First Affiliated Hospital, China Medical University
Xiaoxia Xue
China Medical University
Junying Wu
China Medical University
Fei Li
China Medical University
Dan Song
China Medical University
Xuelian Li (xlli@cmu.edu.cn)
China Medical University

Research Article

Keywords: Hepatocellular carcinoma, Hypoxia-related lncRNAs, Tumor microenvironment, Treatment response, Prognosis

Posted Date: May 11th, 2022

DOI: https://doi.org/10.21203/rs.3.rs-1633183/v1

Abstract

Long non-coding RNAs can regulate hypoxia-induced tumor immune microenvironment remodeling and tumor progression. The present study aimed to build a risk model for predicting the prognosis of hepatocellular carcinoma (HCC) patients based on hypoxia-related lncRNAs and to explore its possible mechanisms. Based on the RNA-Seq and follow-up data downloaded from TCGA and GEO, we performed correlation analysis, differential analysis, and survival analysis to derive candidate hypoxia-related lncRNAs. In total, the 365 patients were used to randomly divide into the training and testing dataset at a ratio of 7:3. The Least Absolute Shrinkage and Selection Operator (Lasso)-Cox regression was applied to select and develop hypoxia-related lncRNAs signature (HRLS) in training datasets. We obtained a risk model consisting of 8 hypoxia-related lncRNAs which was systematically validated in the testing and GSE76427 dataset. HRLS was developed based on SNHG3, NRAV, AC073611.1, AL031985.3, AL049840.6, ZFPM2-AS1, AC074117.1, and MAFG-DT. Patients with low risk displayed a good prognosis, whereas those with high risk had a poor prognosis. Multivariate COX regression analysis also confirmed that the HRLS group was statistically significant after adjusting for clinical factors. Nomogram, time-dependent ROC curve, and decision curve analyses were performed to confirm the predictive ability. Furthermore, the high-risk patients had high-level infiltration of Macrophages and regulatory T cells. Next, AC073611.1 and AL031985.3 were found to be significantly decreased in Hep3B cells after hypoxia exposure (48 hours) in the GSE155505 dataset. Also, the expression of MAFG-DT was significantly upregulated in the sorafenib treatment responders of the GSE109211 dataset. The abnormal expression may be associated with hypoxia states. Finally, we constructed a novel ceRNA network and predicted their binding sites. We developed and validated a novel HRLS to accurately predict patient survival, assess immune infiltration, infer therapeutic benefits, and provide a new perspective for designing personalized therapies.

Introduction

Hepatocellular carcinoma (HCC) is one of the most invasive inflammation-related malignancy, which seriously threatens human health[1]. Epidemiological data revealed there are 906,000 new cases and 830,000 deaths worldwide in 2020[2]. More than 60% of HCC patients are treated primarily based on advanced stages, contributing to limited outcomes and poor prognosis[3]. Currently, surgery and chemotherapy are still considered the first-line clinical treatments for liver cancer. However, continuous chemotherapy can aggravate the hypoxic microenvironment and promote the proliferation of tumor cells, making its long-term efficacy still unsatisfactory. Moreover, high recurrence and metastasis rates can result in a low 5-year overall survival rate[4, 5]. Thus, there is an urgent need to reveal the hypoxia-mediated mechanisms in liver cancer patients to select sensitive treatments and improve prognosis.

Intra-tumoral hypoxia is a crucial feature of all solid tumors, especially HCC. In hypoxic conditions, the cells adapt to low oxygen levels via the hypoxia-inducible factors (HIF) pathway[6]. Meanwhile, HIFs could impact the expression of multiple genes and many malignant phenotypes, including invasiveness, metabolic reprogramming, stem cell maintenance, cell survival and proliferation, immune response, angiogenesis, and chemoresistance[7-9]. To date, the effects of hypoxia on immunosuppression are

receiving widespread attention. Previous studies have discovered that hypoxia reconstructs the tumor microenvironment (TME) and leads to new types of immunogenic cell death, effecting components of both the natural and the acquired immune cells [10].

Currently, with the completion of the Human Genome Project and the establishment of high-throughput genomic technologies, more and more lncRNAs have been identified and their role in tumor diseases has gradually been illuminated. lncRNAs are non-protein-coding transcripts exceeding a length of 200 nucleotides, which exert critical action in the initiation and progression of tumors. Furthermore, it was reported that lincRNA-ROR, ZFPM2-AS1, and HOTAIR can promote proliferation, invasion, metastasis, and chemoresistance of HCC cells[11-13]. Recent studies have found that NRAL regulates Nrf2 expression through miR-340-5p based on a competing endogenous RNA (ceRNA) mechanism, thereby influencing the phenotype of HCC and mediating cisplatin resistance.[14]. However, the systematic identification of existing candidate lncRNAs, especially those associated with hypoxia in the tumor, is still at an early stage and needs further research to be done.

Here, we developed and validated HRLS to predict patients' prognosis, and to contrast immune cell changes, drug sensitivity, and immunotherapy response, which may guide precise treatment. Finally, we constructed a hypoxia-associated ceRNA network in liver cancer and explored lncRNA-miRNA-mRNA binding sites, which suggested new perspectives in understanding the disease mechanism in biological pathways.

Materials And Methods

1. Data preprocessing

The FPKM RNA-seq and follow-up information of 374 HCC patients and 50 healthy controls were retrieved from The Cancer Genome Atlas-Liver Hepatocellular Carcinoma (TCGA-LIHC) (https://portal.gdc.cancer.gov/). The genomic information was reannotated according to the ENSEMBL database and converted into lncRNAs and mRNAs. Nine out of 374 patients were removed due to a lack of information on overall survival (OS) (or zero value), and 365 patients with available clinical data were sorted into standardized data for subsequent analysis. In total, 365 HCC patients were randomly split into the training (247 samples) or test dataset (118 samples) at the ratio of 7:3 for integrated analysis by the caret package. The baseline characteristics were presented in Table 1.

An independent dataset (GSE76427-GPL10558) from the Gene Expression Omnibus database (GEO) (https://www.ncbi.nlm.nih.gov/geo/) was used as external validation, which contained 115 samples of HCC. The lncRNA-sequencing of Human HCC cell lines was obtained from GSE155505 (with 6 samples of Hep3B cells under normoxia and hypoxia for 48h). In GSE109211, there were 21 sorafenib responders and 46 non-responders. In microarray analysis, based on the corresponding annotation file, probe IDs are mapped to gene symbols and expression measurements for all probes associated with the same gene are obtained at an average value. Then, batch normalization was implemented using the sva and limma

package. Moreover, 200 hypoxia-related genes were obtained from the hallmark gene sets of the Molecular Signatures Database (https://www.gsea-msigdb. org/gsea/msigdb/index.jsp).

2. Identification of hypoxia-related lncRNAs

By calculating Pearson correlation coefficients between hypoxia gene and lncRNA expression levels, we identified hypoxia-related lncRNAs in HCC samples. (|r| > 0.4, P-value < 0.001). Ultimately, 486 hypoxia-related lncRNAs were identified using the above criteria in the TCGA-LIHC cohort.

3. Constitution of risk model

The limma algorithm was identified differentially expressed lncRNAs (DElncRNAs) between HCC and adjacent nontumor tissues, and |log Fold-Change| > 1 and False Discovery Rate (FDR) < 0.05 were considered significant differences. These DElncRNAs were visualized by volcano plot. Meanwhile, Univariate analysis was used to filter all hypoxia-related lncRNAs for prognosis-associated lncRNAs, which was provided in the survival and survminer packages (P-value < 0.01). DElncRNAs and prognosis-associated lncRNAs were taken to intersect as candidate lncRNAs.

Subsequently, the candidate lncRNAs were used as an input in the Lasso model[15] by the glmnet package, in which all intersections lncRNAs were penalized to prevent overfitting. The penalty parameter (λ) was set at 10-fold cross-validation in the model. Afterward, the hub-lncRNAs constituted a risk model for identifying hypoxia signatures and generated risk scores as follows:

$$Risk\ score = \sum_{i=1}^{n} Coef(i) * (X)_i$$

Where $Coef(i)$ represented its corresponding coefficient and $(X)_i$ was the lncRNAs expression.

The threshold was defined by median risk score. The survival model was developed based on training datasets. The testing and external dataset were used to validate the HRLS.

4. Prediction of HRLS in the training and validation dataset

To compare the OS between HRLS groups, the Kaplan-Meier method was implemented by survival and survminer packages. Log-rank tests were employed to calculate the difference in survival distributions between two subgroups. After that, the risk score and clinicopathology from three datasets were incorporated into univariate and multivariate survival analyses to confirm independent predictors of prognosis. Moreover, patients were stratified according to clinicopathological factors, such as age, gender, grade, and stage. we calculated whether the OS of HCC patients were still significantly different in the entire TCGA dataset. Nomogram, consistency index (C-index), calibration curve, and Area under the ROC curve (AUC) were used to explore exactly the predictive capacity of the HRLS by survivalROC, timeROC, and rms packages. the predictive power was validated in testing and geo datasets. Also,

Decision Curve Analysis (DCA) was captured the clinical efficacy when we try to use complex models as a tool for decision makers[16, 17].

5. Construction and analysis of ceRNA network

Candidate lncRNAs most relevant to HCC were picked to predict miRNAs by the means of StarBase (http://starbase.sysu.edu.cn/) and miRcode (http://www.mircode.org). Then, we explore target mRNAs of miRNAs through the microRNA Data Integration Portal (mirDIP) (http://ophid.utoronto.ca/mirDIP) and TargetScan (http://www.targetscan.org/). We established the ceRNA network according to the negatively regulating target relationships of miRNA-mRNA and miRNA-lncRNA correlation pairs. Besides, Cytoscape software (3.8.2) was used to visualize obtained results.

6. Functional enrichment analysis

Gene set enrichment analysis (GSEA) of differential expressed genes were enriched using GSEA tools with files (msigdb.v7.4.symbols.gmt) as reference. The biological pathways were significantly enriched when nominal P-value (NOM P-value) < 0.05 and FDR < 0.25 after 1000 permutations. The candidate genes were also clustered into various KEGG pathway ontologies using the ClueGO plug-in provided by Cytoscape for visualizing non-redundant biological terms for large gene clusters in a functional grouping network. The biological function of target genes was enriched using the online tool of Metascape.

7. Estimation of immune cells type

The relative immune cell infiltration levels were quantified using single-sample gene-set enrichment analysis (ssGSEA) algorithm, which consists of activated CD8 T cells, activated dendritic cells, natural killer (NK) cells, etc. [18, 19]. Box plots were drawn to demonstrate the difference between the 16 immune infiltrating cells. Spearman correlations were calculated for some immune cells with risk scores, visualized by the ggplot2 package.

8. Prediction of therapeutic sensitivity

We assessed the predictive power of HRLS in response to immunotherapy and six common chemotherapeutic agents. The GDSC database was explored using the pRRophetic algorithm to infer the half-maximal inhibitory concentration (IC50) value, which was normally transformed. Furthermore, the immunotherapy responses in HCC patients were inferred by the tumor immune dysfunction and exclusion (TIDE) score.

9. Statistical analysis

Data analysis and visualization were conducted using R (4.0.5). The KM and log-rank test were applied to detect the difference of survival analysis. Wilcox Test or Student's t-test was employed to compare the expression levels of lncRNAs, infiltration score of immune cells, and IC50 value between two groups. The chi-squared or Fisher's exact test was applied for follow-up data. Pearson analysis was used to evaluate

respectively the corresponding coefficients among lncRNA-miRNA-mRNA. P-value or adjusted p-value less than 0.05 were regarded as statistically significant.

Results

1. Identification and selection of hypoxia-related lncRNAs

The entire work framework is shown in Fig. 1. We extracted 15036 lncRNAs from the TCGA database. At the same time, 199 hypoxia-related genes were available in HCC samples (Table S1). We performed Pearson analysis to calculate coefficients between hypoxic genes and lncRNAs. We defined 486 hypoxia-related lncRNAs with the criteria that coefficient $|r| > 0.4$ and $P < 0.001$. Significant DElncRNAs were identified among HCC compared with adjacent noncancerous tissues. Next, we identified 300 DElncRNAs (11 downregulated and 289 upregulated lncRNAs) using the limma package (absolute log Fold Change value $|LogFC| > 1$, $P < 0.05$). These DElncRNAs were displayed through the volcano plot (Fig. 2A). In addition, univariate analysis screened prognostic lncRNAs from 486 hypoxia-related lncRNAs, and 77 prognostic lncRNAs were obtained ($P < 0.01$, Table S2). The Venn diagram showed the DElncRNAs and their intersection with hypoxia-related prognostic lncRNAs, the 62 candidate lncRNAs were inputted into further analysis (Fig. 2B).

2. Construction and validation of hypoxia-related lncRNAs signature

The model was constructed from training datasets and verified using validation datasets. As 62 candidate lncRNAs might display similar biological roles, we reduced the dimensionality by Lasso-Cox regression analysis. When its lowest value at a $\log(\lambda)=-2.45$, the risk score model generated corresponding coefficients. Finally, eight hypoxia-related lncRNAs were included to develop the model (Fig. 3A, B). Therefore, the formula was: Risk score=SNHG3*0.0046+NRAV*0.0645+AL031985.3*0.0616+AL049840.6*0.0217+ZFPM2-AS1*0.0546+AC074117.1*0.0681+AC073611.1*0.0676+MAFG-DT*0.0005. In GSE76427, only 5 out of 8 lncRNAs were extracted, containing AC074117.1, ZFPM2-AS1, NRAV, SNHG3, MAFG-DT, and then calculate risk scores. Meanwhile, we obtained the best cut-off value using X-tile software, which was confirmed to be 1.601.

Later, in the training dataset, the survival curve indicated that high-risk patients had significantly inferior prognosis ($P < 0.001$) (Fig. 3C). High-risk HCC patients tended to die earlier (Fig S1). The predicted AUC value for 1-, 3- and 5-year OS were 0.767, 0.710, and 0.710, respectively, indicating the good predictive performance of HRLS (Fig. 3D). Consistent with the training dataset, these trends were observed in the test dataset (Fig. 3E, F) and GSE76427 (Fig. 3G, H).

3. Prognostic value of the hypoxia-related lncRNA signature

In the univariate and multivariate Cox regression model, we analyzed five variables that include age (continuous value), gender (male and female), grade (low and high), stage (I/ II and III/ IV), HRLS (low and

high) in three datasets. As shown in Fig. 4A and Fig. S2A, C, the HRLS was an independent predictive biomarker in three datasets (training dataset: hazard ratio (HR) = 4.017, 95% confidence interval (CI) = 2.389-6.755, P < 0.001; test dataset: HR = 3.319, 95% CI = 1.619-6.808, P = 0.001; GSE76427: HR = 3.477, 95% CI = 1.467-8.242, P = 0.005). Further, multivariate analysis indicated that stage and HRLS were still independent risk factors for OS, and HRLS exhibited highest significance in addition to the other existing clinical parameters (training dataset: HR = 4.164, 95%CI = 2.364-7.334, P < 0.001; test dataset: HR = 2.871, 95%CI = 1.361-6.055, P = 0.006; GSE76427: HR = 3.113, 95%CI = 1.284-7.550, P = 0.012. Fig. 4B, Fig. S2B, D). Then, we constructed a nomogram consisting of two meaningful variates in the entire TCGA dataset (Fig. S3A) and GSE76427 (Fig. S3B), which could predict mortality in HCC patients by quantitative scoring methods. The quantified total score is functionally transformed to obtain the survival probability at 1, 3 and 5 years. Furthermore, the calibration plot showed model has better consistency between predicted OS and actual observations, which consistent with the results of the validation dataset (Fig. S3B, D).

As illustrated in Fig.4C, riskScore had a significantly higher C-index (consistency index) than the stage in TCGA datasets. Importantly, the combination of risk score and stage can significantly promote C-index in the TCGA dataset (stage+riskScore C-index:0.705, 95% CI 0.653-0.757). However, the difference in the C statistics was not significant in GSE76427 datasets (stage+riskScore C-index:0.655, 95% CI 0.546-0.765). Finally, the DCA analysis indicated that HRLS and immune cells models added more net benefit than did the clinical characteristics. It also indicated that prediction with all or non-patient schemes is more beneficial when the decision probability based on the nomogram is >0.25 and <0.4 (Fig. 4D). Therefore, this nomogram showed superior clinical usefulness.

Next, to further evaluate the accuracy of HRLS, patients were stratified based on age, gender, pathological grade, and stage. The survival curve showed that patients in the low-risk subgroup had better OS outcomes compared with ones in the high-risk subgroup in the TCGA studies (Table S3**)**. The classifier also identifies significantly different distribution of risk scores among different subgroups. We found that patients with high grades (T3-T4) and advanced stages (III-IV) had a higher risk score (Fig. S4). Nevertheless, there were no survival benefits in the age and gender subgroups. As such, risk scores may be correlated with pathologic parameters for HCC patients.

4. The landscape of immune cells infiltration

To explore whether HRLS assess changes of immune cells in the TME of liver cancer, we depicted their relationships. Hence, the activation level of 29 immune signatures (16 immune cell types and 13 functions) was calculated using the ssGSEA algorithm according to the reference gene set. As shown in Fig. 5A and Fig. S5, the low-risk subgroup had a significantly greater proportion of NK cells and Mast cells. Macrophages and regulatory T cells (Tregs) were more likely to be distributed in the high-risk subgroup. In particular, we also found that hypoxia risk scores were positively associated with the infiltration of two immune cells, including Macrophages and Treg (Macrophages: r = 0.31, P < 0.001; Fig.

5B; Treg: r = 0.21, P < 0.001; Fig. 6C). It suggested that tumor hypoxic signature is associated with immune cells phenotypes.

5. HRLS predicts therapeutic benefits

To further identify HCC patients who can benefit from chemotherapy, we evaluated 6 drugs response in two risk subgroups. The low-risk patients were highly sensitive to the chemotherapeutics Methotrexate (P-value < 0.001, Fig. 6A), Gefitinib (P-value < 0.0025, Fig. 6B), and Docetaxel (P-value < 0.001, Fig.6 C). Our analysis indicated that their chemotherapy response rates were higher. On the contrary, the high-risk patients were highly sensitive to the chemotherapeutics Cisplatin (P-value < 0.001, Fig. 6D), Bexarotene (P-value < 0.001, Fig. 6E), and Gemcitabine (P-value < 0.001, Fig. 6F), which meant that HRLS may be a potential biomarker for chemosensitivity. The results could also explain that the application of these three drugs could result in a poor prognosis for low-risk patients who may have a chemoresistant environment. We retrieved different drug treatments gene sets from MSigDB to perform GSEA. This supports the above results that three-drug resistance pathways were significantly correlated with HRLS (Fig. 6G, Table S4).

The TIDE algorithm has been applied to the clinical efficacy of immunotherapy. Studies showed that a higher TIDE score means less benefit from immune-checkpoint-inhibitor (ICI) treatment due to immune evasion. Our results showed that the TIDE score in tumors with high-HRLS was significantly lower than those in the low-HRLS subgroup, implying a better response to ICI immunotherapy. (Fig. 6H). Besides, a higher TIDE score may predict worse outcomes for ICI treatment. Also, analysis shows that patients in the low-HRLS subgroup had a higher T cell dysfunction (Fig. 6J) and a lower T cell exclusion score (Fig. 6I). Collectively, these data suggested that risk stratification may be useful in assessing the response of HCC patients to immunotherapy.

6. Gene Set and Function Enrichment Analysis

To understand the underlying mechanism about how hypoxia-related lncRNAs affect liver cancer, GSEA was performed and the results were compared in the two groups in TCGA the dataset. Gene sets upregulated in the high-risk subgroup were tumor proliferation, including MTOR signaling pathway, P53 signaling pathway, VEGF signaling pathway, nod like receptor signaling pathway, and pathway in cancer. In contrast, the immune-related pathways were significantly enriched in the low-risk subgroup, which included the PPAR signaling pathway, fatty acid metabolism pathway, drug metabolism cytochrome 450 pathway, complement, and coagulation cascades pathway, glycine serine, and threonine metabolism pathway (Fig. 7A, Table S4). Meantime, to further investigate the BPs associated with 816 differentially expressed genes corresponding to the HRLS (|LogFC| > 1 and P < 0.05), ClueGO analysis was carried out and suggested that the hypoxia environment was related to four significant GO pathways (P < 0.05), such as cytokine-mediated signaling pathway, icosanoid metabolic process, mitotic spindle organization, and regulation of cell migration (Fig. 7B). These differential genes suggested that hypoxia correlates with oncogenic pathways and enhanced immune function.

7. Validation of the expression level of hypoxia-related lncRNAs and construction of the ceRNA network

We detected the expression level of hub-lncRNAs of 3 hypoxia-treated and 3 normoxia-treated HCC cell lines in the GSE155505 database. The expression of two lncRNAs were significantly decreased in Hep3B cells after hypoxia exposure (48 hours) as compared to the control group, such as AC073611.1 (P = 0.026), AL031985.3 (P = 0.029) (Fig. 8A, B). Therefore, hub-lncRNAs are hypoxia-responsive in HCC cells. Moreover, by calculating the risk score for 67 HCC patients with sorafenib treatment downloaded from the GSE109211 dataset, we found that the expression levels of MAFG-DT (P = 0.00021) were significantly higher in 21 sorafenib treatment responders than in 46 non-responders (Fig. 8C). Taken together, our analyses indicated that the expression level of a single lncRNA may be different in treatment response.

To investigate how hypoxia-associated lncRNAs regulate mRNA expression through sponging miRNAs, we firstly extracted three of 62 lncRNAs from the Starbase and identified 10 pairs of interaction between the three lncRNAs and eight miRNAs. Then, the targets genes of eight candidate miRNAs were obtained via the mirDIP database with the predicted score as 'very high', and total, of 21 mRNAs were identified. Ultimately, based on the above evidence (Table S5, 6), we next constructed a ceRNA regulatory network, which contained 32 nodes and 43 edges (Fig. 8D). Since all three lncRNAs inhibit miR-139 expression, we predicted its binding sites by mircode and TargetScan (Table S7 and S8). In addition, functional analysis of these 21 target genes was implemented by the Metascape online tool. And these genes were found to be associated with the pathways, such as blood vessel development, response to hypoxia, PI3K-Akt-mTOR-signaling pathway, etc. (Fig. 8E-G).

Discussion

Hypoxia is prominent in solid tumors and a recognized driver of malignancy, especially in HCC[20]. Under hypoxic conditions, target genes can be sequentially activated by HIF-α, thereby promoting tumor-specific activities[21]. Emerging evidence indicates that lncRNAs are involved in mediating the biological functions of hypoxia[22, 23]. For example, knockdown of HOTAIR inhibits glycolysis by modulating miR-130a-3p and HIF1A in hypoxia-treated HCC cells, elucidating a novel mechanism in HCC glycolysis[24]. Although novel signatures based on many kinds of cancers (bladder cancer, Gastric Cancer, Clear Cell Renal Carcinoma, etc.) have been described to predict prognostic value, limited success has been achieved due to moderate accuracy or lack of clinical application. [25–27]. Tang et al. developed a hypoxia-related lncRNAs signature which showed better prediction for clinical outcomes of HCC patients, while the associated mechanism remains unclear[28]. Therefore, exploring comprehensively prognostic signatures of liver cancer can effectively guide clinical practice in the future.

In our research, based on eight optimal lncRNAs, the risk score model was capable of stratifying patients into two risk groups. High hypoxic risk patients have a tendency for worse prognosis in training datasets. Furthermore, the KM survival analysis from the testing and GSE76427 datasets also validated the good reproducibility and robustness of the HRLS in predicting patients' prognosis. In addition, the AUC value in the three datasets showed good predictive power. Next, we studied each lncRNA among our identified lncRNAs and found that SNHG3, NRAV, AL031985.3, AC074117.1, MAFG-DT, and AC073611.1 were reported in HCC prognostic signatures, like immune-related lncRNA signature[29–31], glycolysis-related

signature[32], and pyroptosis-related signature[33]. In addition, ZFPM2-AS1 has been found to be closely associated with proliferation, apoptosis, and other similar pathways, such as mTOR, PI3K/AKT, and reactive oxygen species. Mechanistically, ZFPM2-AS1 could attenuate the p53 pathway by regulating miR-139/GDF10[12]. AL049840.6 has not been reported to relate to HCC biology. Thus, the functions and mechanisms of these hypoxia-related lncRNAs in HCC need to be further investigated.

After adjusting for traditional clinical factors, the univariate and multivariate analysis on three datasets also showed that the HRLS group remained an independent prognostic indicator. Based on existing results, we included stage and risk scores to bulid a nomogram model, which extrapolate the survival probability for HCC patients for up to 5 years and customize treatment strategies to prolong survival. The calibration curves reflected that the nomograms can accurately predict the clinical prognosis. The results of the C-index also show that the nomogram has a satisfactory discriminatory power. Specially, decision curve analysis further proved that the HRLS and immune cells have a better net benefit rate than the clinical characteristics. The stratified analysis confirmed that the HRLS accurately evaluated the OS of HCC patients. These patients with higher tumor grades and advanced stages usually have worse survival outcomes [34], which is similar to our results.

Previous studies suggest that the hypoxic microenvironment drives immune suppression through multiple mechanisms. Mechanistically, hypoxia (predominantly via HIF signaling) suppresses the innate and adaptive immune systems to evade immune attack by inducing the expression of immunosuppressive factors and immune checkpoint molecules, including vascular endothelial growth factor, prostaglandin E2 and programmed death-ligand 1/programmed death-1[35, 36]. In addition, Metabolic adaptations of tumor cells to hypoxia, such as increased glucose uptake and lactate production, also promote and perpetuate the immunosuppressive environment[37]. In addition, hypoxic tumors show increased numbers of myeloid-derived suppressor cells (MDSCs), tumor-associated macrophage (TAM), and Tregs, and depressed infiltrating levels of cytotoxic T cells[38]. Meanwhile, Tregs in hypoxia produce extracellular adenosine, which represses effector T-cell function[39]. Similarly, Macrophages and Tregs significantly infiltrated in high-risk score patients, while NK cells and Mast cells infiltrated in low-risk score patients. Our result indicates that there are lower immune activities in high-risk score patients. Further analysis of the potential association between risk level and immune cells, we found that as the hypoxic scores increased, the infiltrating level of two immune cells also increased in the TCGA dataset (Macrophages: $r = 0.31$; Treg: $r = 0.21$). Thus, our results further confirmed that hypoxic levels were positively correlated immunosuppressive environment. However, the mechanisms involved remain unclear.

Next, we explored the chemotherapy benefit in HCC and found that patients with lower risk tended to have higher response rates of Methotrexate, Gefitinib, and Docetaxel. Conversely, the application of Cisplatin, Bexarotene, and Gemcitabine could be more beneficial for patients with higher risk. The TIDE algorithm was developed by Jiang et al. to predict the response to ICI by characterizing dysfunctional T cells and infiltrating cytotoxic T lymphocytes (CTLs) levels[40]. Since a high TIDE score indicated that patients may respond worse to immunotherapy, our analysis revealed that the high-HRLS subgroup had a lower TIDE

score, which meant that patients benefit more from ICI therapy. All of these indicated that HRLS was a potent biomarker for predicting the immunotherapy response. According to this study, combined with the results of the risk score, different patients can choose more sensitive chemotherapy drugs and immunotherapy, singly or in combination. This is more in line with the concept of personalized treatment in precision medicine.

It has been reported that HIF can exacerbate the progression of NAFLD by activating the hepatocyte PPAR-α signaling pathway[41–43]. Hypoxia further exacerbates disease progression in tumors with aberrant PPAR signaling. In glioma samples, PPAR hyperactivation can modulate the immunosuppressive state, which is associated with increased Tregs expression [44]. At the moment, our results of GSEA indicated that oncogenic pathways were significantly enriched in the high-risk subgroup, such as the mTOR signaling pathway, P53 signaling pathway, VEGF signaling pathway, and NOD-like receptor signaling pathway. Meanwhile, the immune-related pathway is mainly enriched in the low-risk subgroup, such as the PPAR signaling pathway, fatty acid metabolism pathway, drug metabolism cytochrome 450 pathway, complement, and coagulation cascades pathway, glycine serine, and threonine metabolism pathway. This suggested that enhanced immunity may improve survival benefits for patients. Furthermore, ClueGO analysis of the differential genes in two HRLS subgroups demonstrated the high relevance of the genes with cell migration and icosanoid metabolic process, etc. Taken together, hypoxia may play a critical modulator in tumorigenesis and progression through these pathways.

Notably, GSE155505 revealed that AC073611.1 and AL031985.3 were downregulated in Hep3B cells under hypoxic conditions respectively. Moreover, GSE109211 suggested that MAFG-DT expression was upregulated in sorafenib treatment responders compared with non-responders. These results are in agreement with previous findings that MAFG-AS1 is upregulated in sorafenib-resistant cells and facilitates the tumor growth and migration by upregulating STRN4 through absorbing miR-3196[45]. Finally, ceRNA regulation networks which consist of three hypoxia-related lncRNAs, eight miRNAs, and twenty-one mRNAs were established for promoting the development of liver cancer under hypoxia.

However, some limitations of current research should be noted. First, although internal and external validation was performed in this study, other independent datasets are needed to further evidence the model. Second, given the complexity of the tumor microenvironment, which is influenced by multiple factors, the interaction between tumor cells and immune infiltration under hypoxic conditions requires more exploration and evidence. Third, future basic trials will be conducted to confirm the binding sites in the ceRNA network.

In summary, the eight hypoxia-related lncRNAs signature developed in this study can allow for accurate prediction of survival of HCC patients. The ability to generate good risk stratification based on hypoxic features could provide additional value beyond traditional pathological parameters and effectively predict the clinical chemotherapeutic drug sensitivity and immunotherapy responses. However, the significance of lncRNAs in the development of HCC is unquestionable, but the mechanisms behind them are unclear and need to be further explored.

Abbreviations

TCGA: The Cancer Genome Atlas; GEO: Gene Expression Omnibus; MSigDB:

Molecular Signatures Database; HCC: Hepatocellular carcinoma; Lasso: Least Absolute Shrinkage and Selection Operator; HRLS: Hypoxia-related lncRNAs signature; HIF: Hypoxia-inducible factors; TME: Tumor microenvironment; ceRNA: competing endogenous RNA; DCA: decision curve analysis; HR: hazard ratio; C-index: concordance index; GSEA: Gene set enrichment analysis; FDR: False Discovery Rate; OS: overall survival; ssGSEA: single-sample gene-set enrichment analysis; TIDE: tumor immune dysfunction and exclusion; Tregs: regulatory T cells; NK: natural killer cells; ICI: immune-checkpoint-inhibitor.

Declarations

Ethics approval and consent to participate

Not applicable.

Consent to publication

Not applicable.

Availability of data and materials

Publicly available datasets were analyzed in this study. This data can be found here: The data of this study were downloaded from TCGA (https://portal.gdc.cancer.gov/repository) and GEO (https://www.ncbi.nlm.nih.gov/geo/) (GSE76427; GSE155505; GSE109211).

Acknowledgments

The authors are grateful to everyone who has participated in this research work.

Funding information

This study was supported by the National Key Research and Development Program of China (No. 2016YFC1302500).

Authors' contributions

Xiugai Li: Research design, Data analysis, Original-draft, Reviewing, and Editing; Chang Zheng: Manuscript preparation, Revisions, Supervision; Xiaoxia Xue: Data analysis and Revisions; Junying Wu, Fei Li, and Dan Song: Chart preparation, Visualization; Xuelian Li: Editing, Supervision, Project administration.

Conflicts of interest

The authors declare that they have no competing interests.

References

1. Piñero F, Dirchwolf M, Pessôa MG. Biomarkers in Hepatocellular Carcinoma: Diagnosis, Prognosis and Treatment Response Assessment. Cells. 2020;9(6). doi:10.3390/cells9061370.
2. Sung H, Ferlay J, Siegel RL, Laversanne M, Soerjomataram I, Jemal A et al. Global Cancer Statistics 2020: GLOBOCAN Estimates of Incidence and Mortality Worldwide for 36 Cancers in 185 Countries. CA: a cancer journal for clinicians. 2021;71(3):209 – 49. doi:10.3322/caac.21660.
3. Yang JD, Hainaut P, Gores GJ, Amadou A, Plymoth A, Roberts LR. A global view of hepatocellular carcinoma: trends, risk, prevention and management. Nat Rev Gastroenterol Hepatol. 2019;16(10):589–604. doi:10.1038/s41575-019-0186-y.
4. Mendez-Blanco C, Fondevila F, Garcia-Palomo A, Gonzalez-Gallego J, Mauriz JL. Sorafenib resistance in hepatocarcinoma: role of hypoxia-inducible factors. Exp Mol Med. 2018;50(10):1–9. doi:10.1038/s12276-018-0159-1.
5. Raoul JL, Forner A, Bolondi L, Cheung TT, Kloeckner R, de Baere T. Updated use of TACE for hepatocellular carcinoma treatment: How and when to use it based on clinical evidence. Cancer treatment reviews. 2019;72:28–36. doi:10.1016/j.ctrv.2018.11.002.
6. Guo Y, Xiao Z, Yang L, Gao Y, Zhu Q, Hu L et al. Hypoxia inducible factors in hepatocellular carcinoma (Review). Oncol Rep. 2020;43(1):3–15. doi:10.3892/or.2019.7397.
7. Du Y, Wei N, Ma R, Jiang SH, Song D. Long Noncoding RNA MIR210HG Promotes the Warburg Effect and Tumor Growth by Enhancing HIF-1α Translation in Triple-Negative Breast Cancer. Front Oncol. 2020;10:580176. doi:10.3389/fonc.2020.580176.
8. Luo X, Li A, Chi X, Lin Y, Liu X, Zhang L et al. Hypoxia-Activated Prodrug Enabling Synchronous Chemotherapy and HIF-1α Downregulation for Tumor Treatment. Bioconjugate chemistry. 2021;32(5):983–90. doi:10.1021/acs.bioconjchem.1c00131.
9. Mortezaee K, Majidpoor J. The impact of hypoxia on immune state in cancer. Life sciences. 2021;286:120057. doi:10.1016/j.lfs.2021.120057.
10. Vito A, El-Sayes N, Mossman K. Hypoxia-Driven Immune Escape in the Tumor Microenvironment. Cells. 2020;9(4). doi:10.3390/cells9040992.
11. Li C, Lu L, Feng B, Zhang K, Han S, Hou D et al. The lincRNA-ROR/miR-145 axis promotes invasion and metastasis in hepatocellular carcinoma via induction of epithelial-mesenchymal transition by targeting ZEB2. Scientific reports. 2017;7(1):4637. doi:10.1038/s41598-017-04113-w.
12. He H, Wang Y, Ye P, Yi D, Cheng Y, Tang H et al. Long noncoding RNA ZFPM2-AS1 acts as a miRNA sponge and promotes cell invasion through regulation of miR-139/GDF10 in hepatocellular carcinoma. J Exp Clin Cancer Res. 2020;39(1):159. doi:10.1186/s13046-020-01664-1.

13. Zhou JJ, Cheng D, He XY, Meng Z, Ye HL, Chen RF. Knockdown of long non-coding RNA HOTAIR sensitizes hepatocellular carcinoma cell to cisplatin by suppressing the STAT3/ABCB1 signaling pathway. Oncol Lett. 2017;14(6):7986–92. doi:10.3892/ol.2017.7237.
14. Wu LL, Cai WP, Lei X, Shi KQ, Lin XY, Shi L. NRAL mediates cisplatin resistance in hepatocellular carcinoma via miR-340-5p/Nrf2 axis. J Cell Commun Signal. 2019;13(1):99–112. doi:10.1007/s12079-018-0479-x.
15. Gao J, Kwan PW, Shi D. Sparse kernel learning with LASSO and Bayesian inference algorithm. Neural networks: the official journal of the International Neural Network Society. 2010;23(2):257–64. doi:10.1016/j.neunet.2009.07.001.
16. Vickers AJ, Cronin AM, Elkin EB, Gonen M. Extensions to decision curve analysis, a novel method for evaluating diagnostic tests, prediction models and molecular markers. BMC Med Inform Decis Mak. 2008;8:53. doi:10.1186/1472-6947-8-53.
17. Kerr KF, Brown MD, Zhu K, Janes H. Assessing the Clinical Impact of Risk Prediction Models With Decision Curves: Guidance for Correct Interpretation and Appropriate Use. J Clin Oncol. 2016;34(21):2534–40. doi:10.1200/JCO.2015.65.5654.
18. Bindea G, Mlecnik B, Tosolini M, Kirilovsky A, Waldner M, Obenauf AC et al. Spatiotemporal dynamics of intratumoral immune cells reveal the immune landscape in human cancer. Immunity. 2013;39(4):782–95. doi:10.1016/j.immuni.2013.10.003.
19. Charoentong P, Finotello F, Angelova M, Mayer C, Efremova M, Rieder D et al. Pan-cancer Immunogenomic Analyses Reveal Genotype-Immunophenotype Relationships and Predictors of Response to Checkpoint Blockade. Cell reports. 2017;18(1):248–62. doi:10.1016/j.celrep.2016.12.019.
20. Schneider MA, Linecker M, Fritsch R, Muehlematter UJ, Stocker D, Pestalozzi B et al. Phase Ib dose-escalation study of the hypoxia-modifier Myo-inositol trispyrophosphate in patients with hepatopancreatobiliary tumors. Nature communications. 2021;12(1):3807. doi:10.1038/s41467-021-24069-w.
21. Li T, Mao C, Wang X, Shi Y, Tao Y. Epigenetic crosstalk between hypoxia and tumor driven by HIF regulation. J Exp Clin Cancer Res. 2020;39(1):224. doi:10.1186/s13046-020-01733-5.
22. Huan L, Guo T, Wu Y, Xu L, Huang S, Xu Y et al. Hypoxia induced LUCAT1/PTBP1 axis modulates cancer cell viability and chemotherapy response. Molecular cancer. 2020;19(1):11. doi:10.1186/s12943-019-1122-z.
23. Liang Y, Song X, Li Y, Chen B, Zhao W, Wang L et al. LncRNA BCRT1 promotes breast cancer progression by targeting miR-1303/PTBP3 axis. Molecular cancer. 2020;19(1):85. doi:10.1186/s12943-020-01206-5.
24. Hu M, Fu Q, Jing C, Zhang X, Qin T, Pan Y. LncRNA HOTAIR knockdown inhibits glycolysis by regulating miR-130a-3p/HIF1A in hepatocellular carcinoma under hypoxia. Biomed Pharmacother. 2020;125:109703. doi:10.1016/j.biopha.2019.109703.

25. Chen Q, Hu L, Chen K. Construction of a Nomogram Based on a Hypoxia-Related lncRNA Signature to Improve the Prediction of Gastric Cancer Prognosis. Front Genet. 2020;11:570325. doi:10.3389/fgene.2020.570325.
26. Zhang F, Wang X, Hu H, Yang Y, Wang J, Tang Y et al. A hypoxia related long non-coding RNA signature could accurately predict survival outcomes in patients with bladder cancer. Bioengineered. 2021;12(1):3802–23. doi:10.1080/21655979.2021.1948781.
27. Zhang H, Qin C, Liu HW, Guo X, Gan H. An Effective Hypoxia-Related Long Non-Coding RNAs Assessment Model for Prognosis of Clear Cell Renal Carcinoma. Front Oncol. 2021;11:616722. doi:10.3389/fonc.2021.616722.
28. Tang P, Qu W, Wang T, Liu M, Wu D, Tan L et al. Identifying a Hypoxia-Related Long Non-Coding RNAs Signature to Improve the Prediction of Prognosis and Immunotherapy Response in Hepatocellular Carcinoma. Front Genet. 2021;12:785185. doi:10.3389/fgene.2021.785185.
29. Zhou P, Lu Y, Zhang Y, Wang L. Construction of an Immune-Related Six-lncRNA Signature to Predict the Outcomes, Immune Cell Infiltration, and Immunotherapy Response in Patients With Hepatocellular Carcinoma. Front Oncol. 2021;11:661758. doi:10.3389/fonc.2021.661758.
30. Chen ZA, Tian H, Yao DM, Zhang Y, Feng ZJ, Yang CJ. Identification of a Ferroptosis-Related Signature Model Including mRNAs and lncRNAs for Predicting Prognosis and Immune Activity in Hepatocellular Carcinoma. Front Oncol. 2021;11:738477. doi:10.3389/fonc.2021.738477.
31. Kong W, Wang X, Zuo X, Mao Z, Cheng Y, Chen W. Development and Validation of an Immune-Related lncRNA Signature for Predicting the Prognosis of Hepatocellular Carcinoma. Front Genet. 2020;11:1037. doi:10.3389/fgene.2020.01037.
32. Xia X, Zhang H, Xia P, Zhu Y, Liu J, Xu K et al. Identification of Glycolysis-Related lncRNAs and the Novel lncRNA WAC-AS1 Promotes Glycolysis and Tumor Progression in Hepatocellular Carcinoma. Front Oncol. 2021;11:733595. doi:10.3389/fonc.2021.733595.
33. Wu ZH, Li ZW, Yang DL, Liu J. Development and Validation of a Pyroptosis-Related Long Non-coding RNA Signature for Hepatocellular Carcinoma. Frontiers in cell and developmental biology. 2021;9:713925. doi:10.3389/fcell.2021.713925.
34. Huo J, Fan X, Qi B, Sun P. A Five-Gene Signature Associated With DNA Damage Repair Molecular Subtype Predict Overall Survival for Hepatocellular Carcinoma. Front Genet. 2022;13:771819. doi:10.3389/fgene.2022.771819.
35. Kong SK, Kim BS, Lim H, Kim HJ, Kim YS. Dissection of PD-L1 promoter reveals differential transcriptional regulation of PD-L1 in VHL mutant clear cell renal cell carcinoma. Laboratory investigation; a journal of technical methods and pathology. 2022;102(4):352–62. doi:10.1038/s41374-021-00703-5.
36. You L, Wu W, Wang X, Fang L, Adam V, Nepovimova E et al. The role of hypoxia-inducible factor 1 in tumor immune evasion. Medicinal research reviews. 2021;41(3):1622–43. doi:10.1002/med.21771.
37. Hao X, Ren Y, Feng M, Wang Q, Wang Y. Metabolic reprogramming due to hypoxia in pancreatic cancer: Implications for tumor formation, immunity, and more. Biomed Pharmacother.

2021;141:111798. doi:10.1016/j.biopha.2021.111798.

38. Eckert F, Zwirner K, Boeke S, Thorwarth D, Zips D, Huber SM. Rationale for Combining Radiotherapy and Immune Checkpoint Inhibition for Patients With Hypoxic Tumors. Frontiers in immunology. 2019;10:407. doi:10.3389/fimmu.2019.00407.
39. Jarvis LB, Rainbow DB, Coppard V, Howlett SK, Georgieva Z, Davies JL et al. Therapeutically expanded human regulatory T-cells are super-suppressive due to HIF1A induced expression of CD73. Communications biology. 2021;4(1):1186. doi:10.1038/s42003-021-02721-x.
40. Jiang P, Gu S, Pan D, Fu J, Sahu A, Hu X et al. Signatures of T cell dysfunction and exclusion predict cancer immunotherapy response. Nature medicine. 2018;24(10):1550–8. doi:10.1038/s41591-018-0136-1.
41. He Y, Yang W, Gan L, Liu S, Ni Q, Bi Y et al. Silencing HIF-1α aggravates non-alcoholic fatty liver disease in vitro through inhibiting PPAR-α/ANGPTL4 singling pathway. Gastroenterologia y hepatologia. 2021;44(5):355–65. doi:10.1016/j.gastrohep.2020.09.014.
42. Chen J, Chen J, Fu H, Li Y, Wang L, Luo S et al. Hypoxia exacerbates nonalcoholic fatty liver disease via the HIF-2α/PPARα pathway. American journal of physiology Endocrinology and metabolism. 2019;317(4):E710-e22. doi:10.1152/ajpendo.00052.2019.
43. Mooli RGR, Rodriguez J, Takahashi S, Solanki S, Gonzalez FJ, Ramakrishnan SK et al. Hypoxia via ERK Signaling Inhibits Hepatic PPARα to Promote Fatty Liver. Cellular and molecular gastroenterology and hepatology. 2021;12(2):585–97. doi:10.1016/j.jcmgh.2021.03.011.
44. Chang WH, Lai AG. The pan-cancer mutational landscape of the PPAR pathway reveals universal patterns of dysregulated metabolism and interactions with tumor immunity and hypoxia. Annals of the New York Academy of Sciences. 2019;1448(1):65–82. doi:10.1111/nyas.14170.
45. Chen T, Huang B, Pan Y. Long Non-coding RNA MAFG-AS1 Promotes Cell Proliferation, Migration, and EMT by miR-3196/STRN4 in Drug-Resistant Cells of Liver Cancer. Frontiers in cell and developmental biology. 2021;9:688603. doi:10.3389/fcell.2021.688603.

Tables

Table1. Baseline Clinical Characteristic of TCGA Database

Characteristics	Training cohort (N=247)	Testing cohort (N=118)	P-value
Age at diagnosis(years)			
<=65	152(41.64%)	75(20.55%)	0.80
>65	95(26.03%)	43(11.78%)	
Gender			
Male	85(23.29%)	34(9.32%)	0.34
Female	162(44.38%)	84(23.01%)	
Histological grade	5 missing		
Low grade	150(41.67%)	80(22.22%)	0.27
High grade	93(25.83%)	37(10.28%)	
AJCC-stage	24 missing		
Stage I	115(33.72%)	55(16.13%)	0.86
Stage II	57(16.72%)	27(7.92%)	
Stage III	58(17.01%)	25(7.33%)	
Stage IV	2(0.59%)	2(0.59%)	

*Chi-square test

Figures

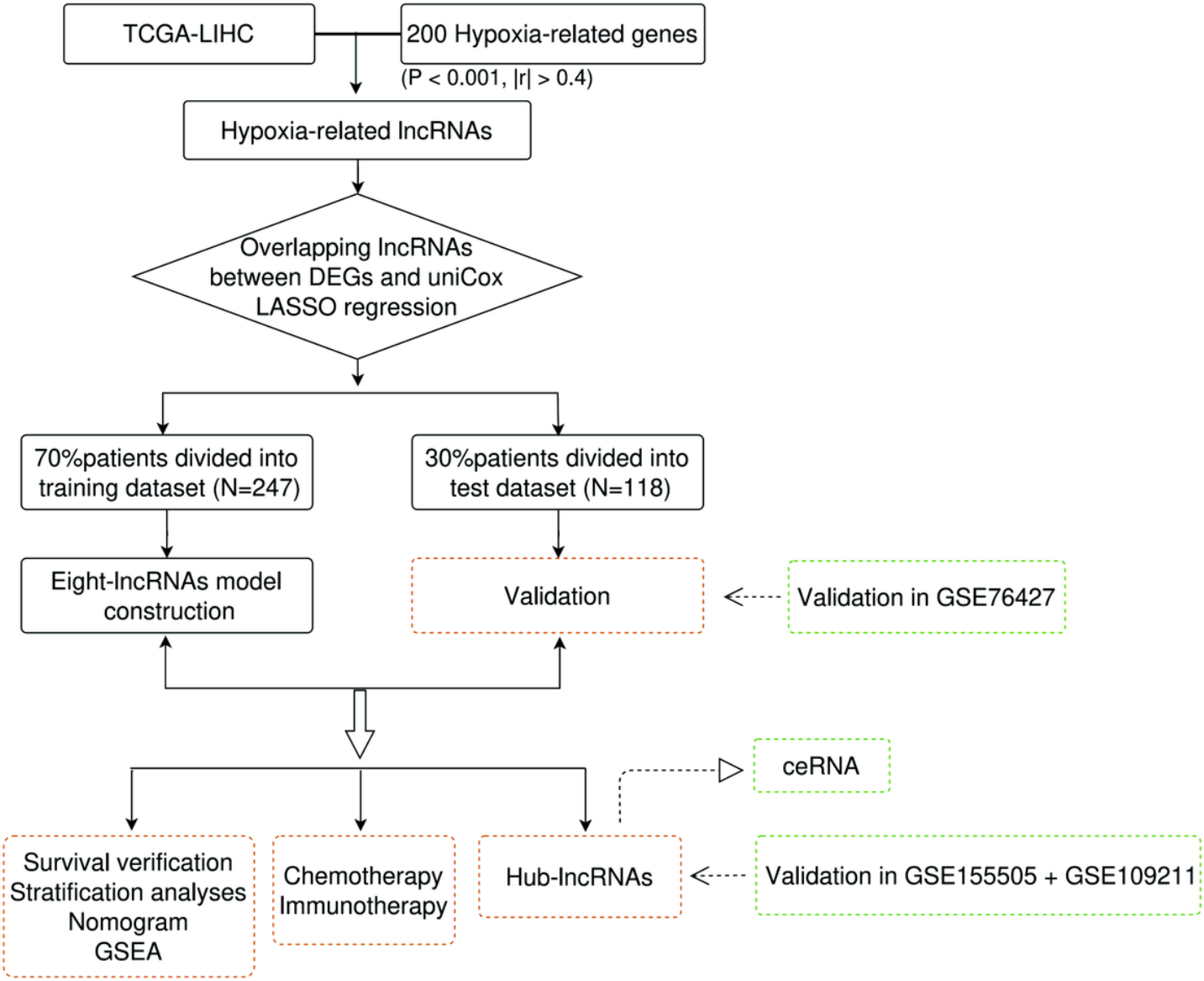

Figure 1

The workflow of the research.

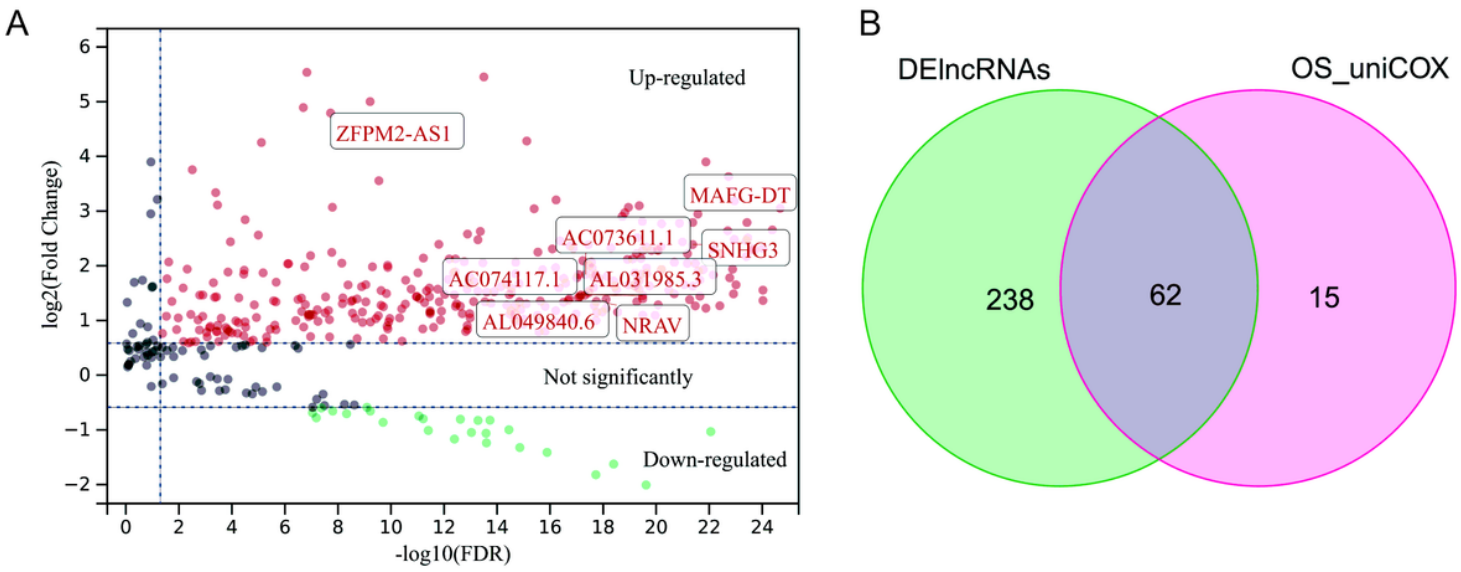

Figure 2

Identification and selection of hypoxia-related lncRNAs in HCC.

A Differentially expressed analysis in the HCC and adjacent noncancerous tissues. **B** Venn plot shows the number of intersection-lncRNAs between DElncRNAs and prognostic lncRNAs.

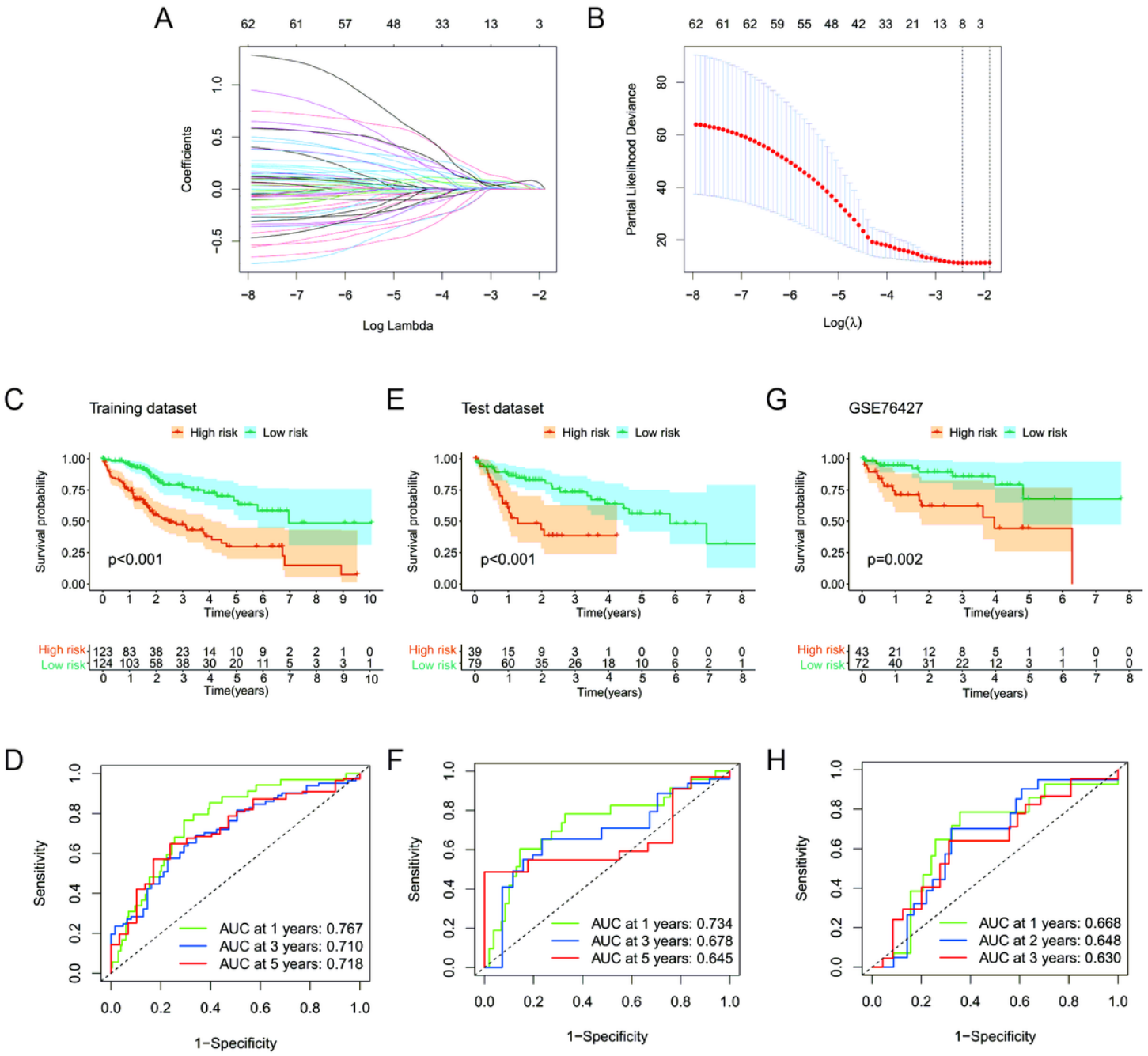

Figure 3

Construction and validation of hypoxia risk model in HCC.

A, B The Lasso-Cox regression model to identify the most robust lncRNAs. **C, E, G** Kaplan-Meier analysis showed that patients with lower risk scores had better overall survival than the ones with higher risk scores in the training, test, and GSE76427 dataset. **D, F, H** Verification of the prognostic value of the hypoxia-related lncRNA signature by ROC analysis in the training, test, and GSE76427 dataset.

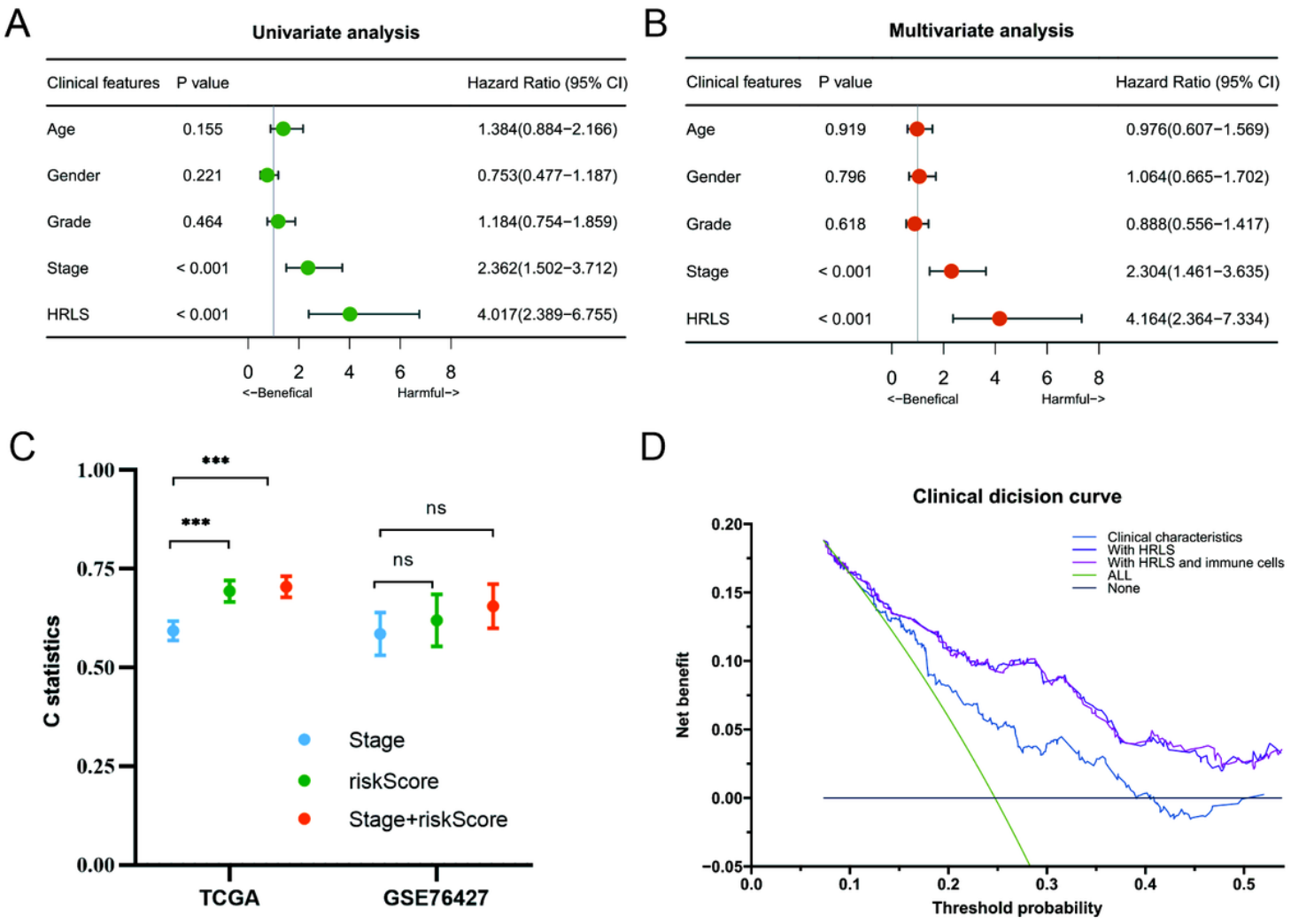

Figure 4

Evaluation and validation for the prognostic value of the HRLS.

A, B The univariate and multivariate Cox regression suggested that the risk score was an independent prognostic factor in the training set. **C** C-statistics of stage and riskScore in TCGA and GSE76427. **D** Comparisons of the clinical utility for the clinical variables, combined with a tumor risk score, and combined with both tumor risk score and immune cells using decision curve in the entire TCGA dataset.

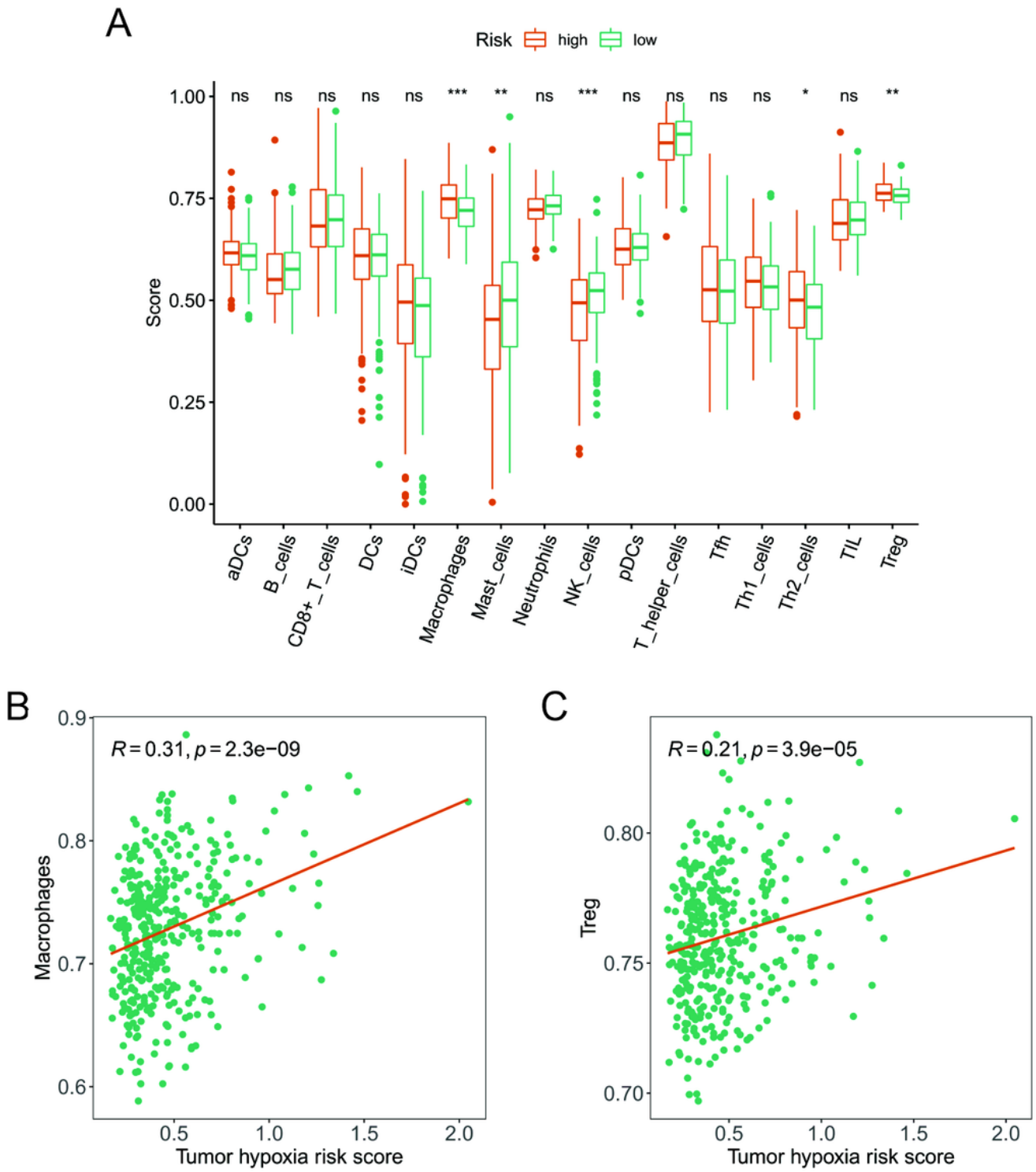

Figure 5

Tumor-infiltrating immune cells of HCC patients.

A Comparison of ssGSEA scores of 16 immune cells between high and low risk group in TCGA. ****, p < 0.0001; ***, p < 0.001; **, p < 0.01; *, p < 0.05; ns: no significance. Correlation of tumor hypoxia score as expression with **B** Macrophages and **C** Treg.

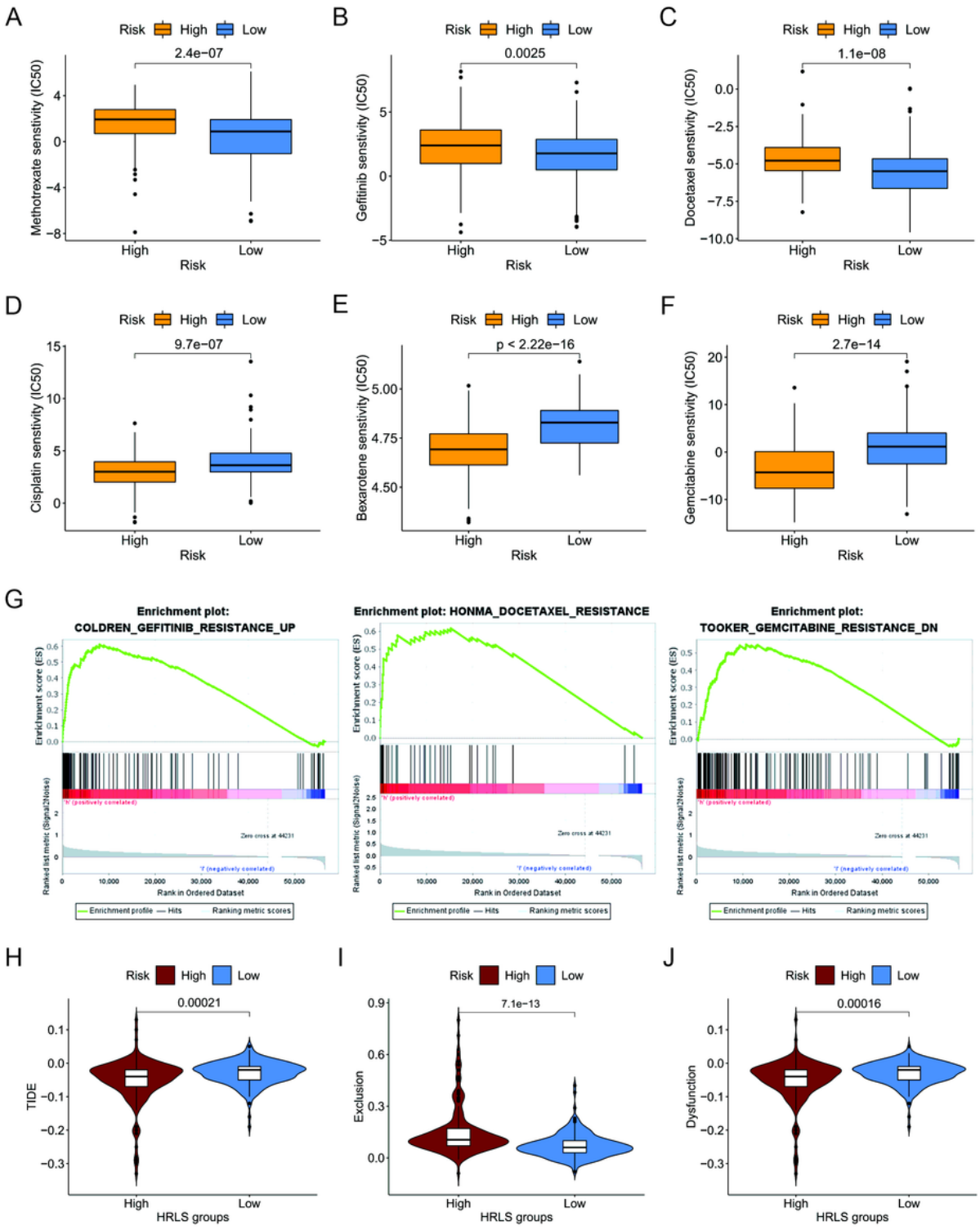

Figure 6

HRLS predict therapeutic response in HCC patients.

A-F Relationship between different risk score subgroups and six common chemotherapy drugs. **G** GSEA showed that coldren_gefitinib_resistance_up, honma_docetaxel_resistance, and

tooker_gemcitabine_resistance_dn are enriched in the high-risk group. TIDE score **(H),** T cell exclusion score **(I),** and T cell dysfunction score **(J)** between different risk score subgroups.

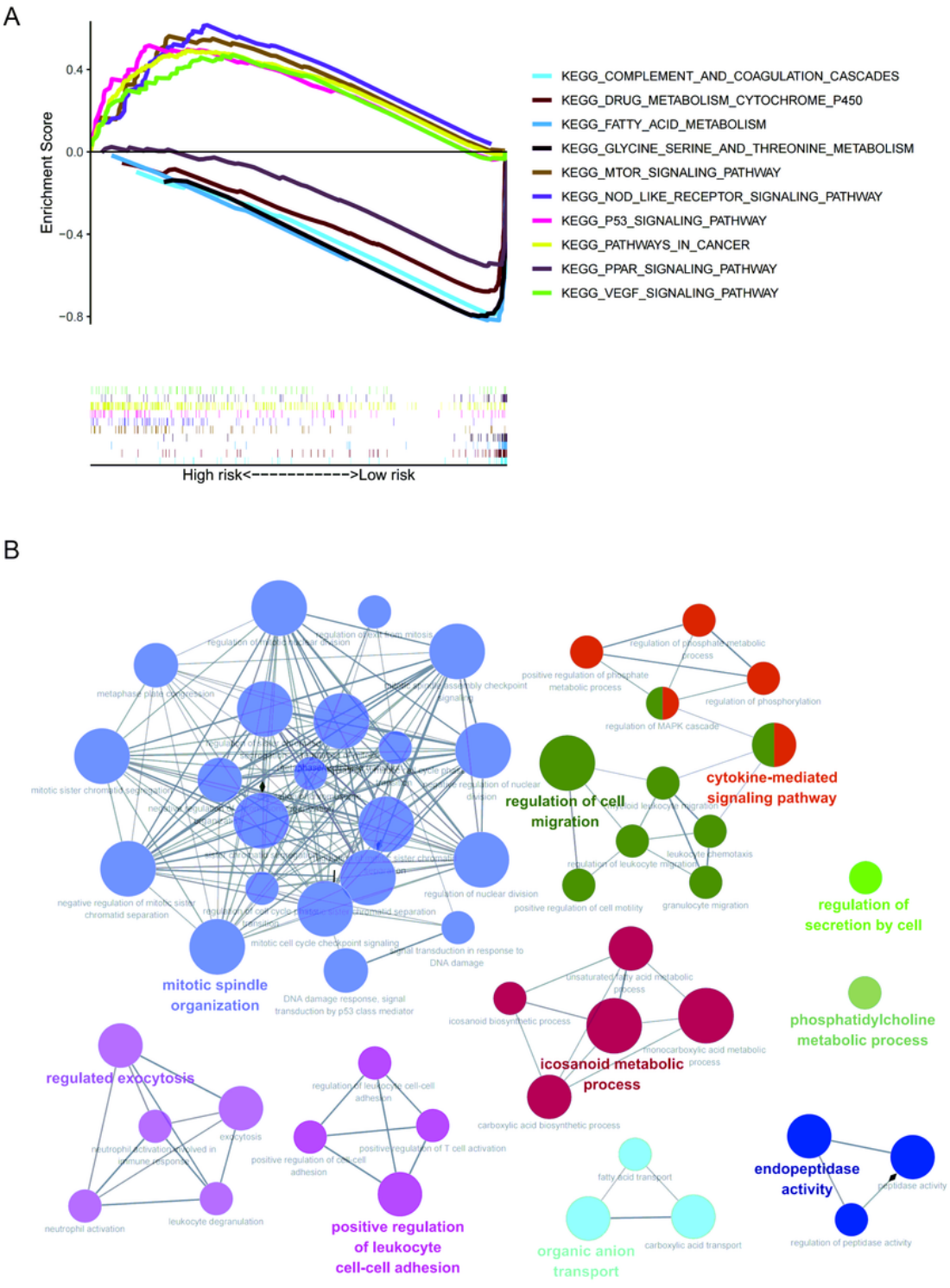

Figure 7

Function enrichment analysis.

A GSEA results showed differential enrichment of genes in KEGG with hypoxia-related lncRNA expression. (5 KEGG items namely, MTOR signaling pathway, P53 signaling pathway, VEGF signaling pathway, nod like receptor signaling pathway, and pathway in cancer were significantly differential enrichment in high expression phenotype; 5 KEGG items namely, PPAR signaling pathway, fatty acid metabolism pathway, drug metabolism cytochrome 450 pathway, complement, and coagulation cascades pathway, glycine serine and threonine metabolism pathway showed significantly differential enrichment in the hypoxia-related lncRNA low-expression phenotype based on the normalized enrichment score (NES), nominal p-value (NOM P-value), and FDR value). **B** The small size nodes in the network represent the genes enriched in the specific pathway, the big size nodes represent the pathway term. The node colors correspond to the ClueGO-determined KEGG pathway clusters.

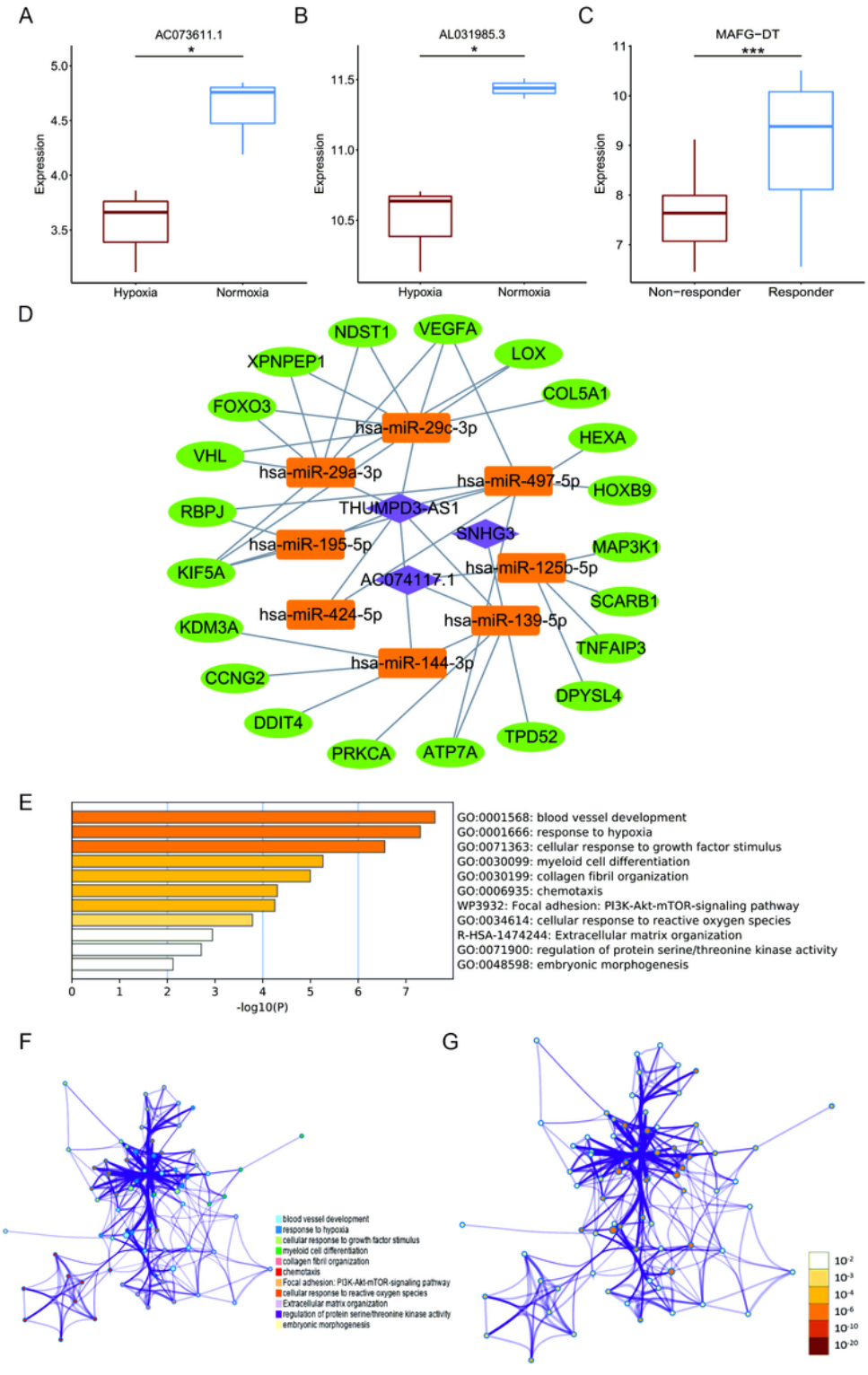

Figure 8

The expression levels of hub lncRNAs in liver cancer cell lines and construction of the ceRNA network.

AB Differences in expression between the hypoxia and normoxia in GSE155505. **C** Difference of expression between sorafenib treatment responders and nonresponders. *p < 0.05, **p < 0.01, ***p < 0.001, ****p < 0.0001. **D** lncRNA-miRNA-mRNA ceRNA network in HCC. Purple, orange, and green

represent lncRNAs, miRNAs, and mRNAs, respectively. **E** Heatmap of enriched terms across the twenty-one mRNAs, colored according to the p-value. Network of enriched terms colored according to (**F**) cluster ID (nodes with the same cluster-ID are typically close to each other) and (**G**) p-value (terms with more genes tend to have higher p-values).

Supplementary Files

This is a list of supplementary files associated with this preprint. Click to download.

- figS1.tif
- figS2.tif
- figS3.tif
- figS4.tif
- figS5.tif
- SupplementaryallTable.docx